

Beiträge aus der Informationstechnik

Mobile Nachrichtenübertragung

Nr. 96

Peng Huang

**Sensor Fusion for Flight State Estimation of
Fixed-Wing Aerial Vehicles:
Design, Implementation and Analysis**

 VOGT

Dresden 2023

Bibliografische Information der Deutschen Nationalbibliothek
Die Deutsche Nationalbibliothek verzeichnet diese Publikation in der
Deutschen Nationalbibliografie; detaillierte bibliografische Daten sind im
Internet über <http://dnb.dnb.de> abrufbar.

Bibliographic Information published by the Deutsche Nationalbibliothek
The Deutsche Nationalbibliothek lists this publication in the Deutsche
Nationalbibliografie; detailed bibliographic data are available on the Internet
at <http://dnb.dnb.de>.

Zugl.: Dresden, Techn. Univ., Diss., 2022

Die vorliegende Arbeit stimmt mit dem Original der Dissertation
„Sensor Fusion for Flight State Estimation of Fixed-Wing Aerial Vehicles:
Design, Implementation and Analysis“ von Peng Huang überein.

© Jörg Vogt Verlag 2023
Alle Rechte vorbehalten. All rights reserved.

Gesetzt vom Autor

ISBN 978-3-95947-059-9

Jörg Vogt Verlag
Niederwaldstr. 36
01277 Dresden
Germany

Phone: +49-(0)351-31403921
Telefax: +49-(0)351-31403918
e-mail: info@vogtverlag.de
Internet : www.vogtverlag.de

Technische Universität Dresden

**Sensor Fusion for Flight State Estimation of Fixed-Wing Aerial Vehicles:
Design, Implementation and Analysis**

Dipl.-Ing.

Peng Huang

der Fakultät Elektrotechnik und Informationstechnik der Technischen Universität
Dresden

zur Erlangung des akademischen Grades

Doktoringenieur

(Dr.-Ing.)

vorgelegte Dissertation

Vorsitzender:	Prof. Dr.-Ing. habil. Dipl.-Math. Klaus Röbenack
Gutachter:	Prof. Dr.-Ing. Dr. h.c. Gerhard Fettweis Prof. Dr. Sami Haddadin Prof. Dr. Heinrich Meyr

Tag der Einreichung:	07. April 2022
Tag der Verteidigung:	27. September 2022

Abstract

Unmanned and manned aerial vehicles have been used extensively for civilian purposes over the past few decades, thanks to unprecedented advances in micro-electro-mechanical systems (MEMS) sensors and microprocessors. One can find various sensors in aerial vehicles, such as triaxial accelerometers, triaxial gyroscopes, triaxial magnetometers, GPS modules, and pressure sensors. The digital sensor signals are processed in microprocessors using sensor fusion techniques, which provide navigation capabilities for aerial vehicles.

In this thesis, we present an approach of design and implementation of a sensor fusion algorithm for fixed-wing aerial vehicles. The flight state variables of the sensor fusion algorithm are the position, velocity, orientation of the aerial vehicle, biases of an inertial measurement unit (IMU), and wind speed. The state dynamics are nonlinear due to the orientation. Therefore, we propose to apply an extended Kalman filter (EKF) using inertial measurements (acceleration and angular velocity), GPS position, static pressure, dynamic pressure, and air temperature measurements. In addition to these measurements, two aerodynamic constraints (side force and sink rate polar) of a fixed-wing airplane are used for the wind estimation using an assumption of a wind triangle.

We propose not to use magnetic measurements since they are easily distorted by unknown magnetic fields of other electronic devices in the vicinity. The distortion is not well compensated, if at all. Without heading information from the magnetic measurements, the horizontal wind cannot be uniquely determined in a single wind triangle. Therefore, we investigate the wind estimation in the proposed EKF without a magnetic sensor. Using an analytical observability analysis, we prove that the wind is observable in the case of a time-varying true airspeed (TAS) direction, which is commonly fulfilled in practical flights. To this end, a numerical study of the observability of the EKF using measured flight data of a manned glider shows that the state vector is effectively observable independent of flight maneuvers. We show that the EKF works without a magnetometer. Furthermore, in order to study the tracking behavior of the individual state variables, we present a method based on the triangularization of the system transition matrix. We show that the wind estimation error can converge in flights with dynamically changing TAS direction. The TAS direction determines which direction of the wind estimate converges faster.

A further key contribution of this thesis is the experimental evaluation of the proposed EKF using recorded flight measurements in different manned gliders under realistic environmental conditions, e.g., smooth air and turbulent atmospheres. The pilot-in-the-loop strategy allows us to collect and label various flight maneuvers, including gliding, soaring in thermals, uncoordinated turning, stall, and free-fall flight. The results show that the EKF can accurately estimate the position, ground speed, orientation, IMU biases, and wind speed in real-time. The horizontal wind estimate is verified by circle shifting in a thermal soaring of a glider. The vertical wind estimate is instantaneous and accurate and can be used to indicate a strong updraft. In addition, we determine the side force coefficient of the side force model using uncoordinated turnings. As a byproduct, the EKF can estimate the angle of attack using a three-dimensional TAS vector. The AoA estimates are evaluated using two specific flight maneuvers, i.e., stall and free-fall flight.

Statement of authorship

I hereby certify that I have authored this Dissertation entitled *Sensor Fusion for Flight State Estimation of Fixed-Wing Aerial Vehicles: Design, Implementation and Analysis* independently and without undue assistance from third parties. No other than the resources and references indicated in this thesis have been used. I have marked both literal and accordingly adopted quotations as such. There were no additional persons involved in the intellectual preparation of the present thesis. I am aware that violations of this declaration may lead to subsequent withdrawal of the degree.

Peng Huang

Restriction note

This Dissertation entitled *Sensor Fusion for Flight State Estimation of Fixed-Wing Aerial Vehicles: Design, Implementation and Analysis* contains confidential data. Publications, duplications and inspections—even in part—are prohibited without explicit permission, as well as publications about the content of this thesis. This thesis may only be made accessible to the supervisor at Technische Universität Dresden, the reviewers and also the members of the examination board.

Acknowledgement

I would like to express my gratitude to Prof. Gerhard Fettweis for offering me a position at the Vodafone Chair at TU Dresden for his guidance and support on exciting research topics. Special thanks go to Prof. Heinrich Meyr for sharing his experience and expertise in countless scientific discussions. As a glider pilot, he helped collect flight measurements and shared in-depth knowledge about flight results. I am furthermore grateful to Prof. Sami Haddadin for serving as the second reviewer of this thesis.

I would like to thank Dr. Meik Dörpinghaus, who gave me valuable advice on scientific topics and papers. My thanks also go to my CoCoColleagues Arturo, Ketong, Eva, Andres, and Lukas for the fruitful meetings and discussions. I want to thank Mostafa, who raised my interest in sensor fusion during my diploma thesis. Furthermore, I express my thanks to Kathrin and Sylvia for keeping the chair running and for support in any administrative matters.

My special thanks goes to my project partners, Erazem Polutnik and Marko Jelenko from LXNAV. They carried out the experimental tests of the developed algorithm. Moreover, they assisted with their expertise in aerodynamics. They provided avionics hardware on which we integrated our algorithms with their support. I want to express my appreciation to test pilots Klaus Ohlmann, Michael Seischab, Uroš Krašovic, Benjamin Meier, Torben Raatz, Frederic Pflaum, Roland Bieri, and Philipp Keller for their valuable flights and feedback about the flight results.

Finally, I would like to thank my parents for supporting my studies in Germany and always believing in me. My greatest thanks go to my wife, Zhenzhen, for her love, support in good or bad times, and her company that always inspires me and keeps me motivated.

Contents

Abstract	iii
1. Introduction	1
1.1. Motivation	1
1.2. Background	2
1.3. Outline and Contributions	6
2. Sensor Fusion Conceptual Design	11
2.1. Problem Statement	11
2.2. Sensor Fusion Development Paradigm Chosen	13
2.3. HAWK - Sensor Fusion System	17
2.4. Summary	18
3. Multi-Sensor Fusion for State Estimation	21
3.1. Related Work	21
3.2. Prerequisites	22
3.2.1. Coordinate Frames	23
3.2.2. Attitude Representations	24
3.2.3. Aerodynamics Forces	25
3.3. Nonlinear Filtering	26
3.3.1. Nonlinear State-Space Model	26
3.3.2. Extended Kalman Filtering	28
3.4. Multi-Sensor Fusion based on EKF	28
3.4.1. Kinematics and Inertial Sensor Model	29
3.4.2. State Dynamics and Measurement Model	31
3.4.3. The EKF Equations	34
3.5. Estimation Results using Simulated Measurements	43
3.6. Summary	45
4. Observability and Reachability Analysis	49
4.1. Introduction	49
4.2. Related Work	50

4.3.	Observability and Reachability for Nonlinear Systems	51
4.3.1.	Observability	51
4.3.2.	Reachability	54
4.4.	Observability and Reachability Analysis for Simplified 2D EKF	56
4.4.1.	Simplified 2D EKF	56
4.4.2.	Analytical Observability Analysis	57
4.4.3.	Numerical Observability Analysis	59
4.4.4.	Reachability Analysis	62
4.5.	Observability Analysis for Full State EKF	63
4.6.	Summary	65
5.	Dynamic Tracking Behaviour of EKF	67
5.1.	Introduction	67
5.2.	State Error Dynamics of an EKF	68
5.3.	Dynamic Tracking Behavior of LTV Systems	70
5.3.1.	Stability Property	70
5.3.2.	Transient Behavior via System Decomposition	71
5.4.	Simulation Results	79
5.4.1.	Results of the Simplified 2D System	79
5.4.2.	Acquisition Behavior under Perturbations	82
5.5.	Summary	85
6.	Glider Flight Testing	87
6.1.	Introduction	87
6.2.	Determination of Sensor Statistics	90
6.3.	Estimation Results with An Exemplary Gliding Flight	91
6.4.	Turbulence of Wind Velocity Estimates	92
6.5.	Estimation Results during Thermal Soaring	96
6.5.1.	Estimation Results of A typical Thermal Soaring	97
6.5.2.	Response Time of Updraft Indication	100
6.6.	Estimation Results of Uncoordinated Turn	100
6.6.1.	Selection of Side Force Coefficient	102
6.6.2.	Effects of Uncoordinated Turn	103
6.7.	Angle of Attack Estimation Evaluation	105
6.8.	Test Pilots and Flights	107
6.9.	Summary	107
7.	Conclusions and Future Work	109
	Appendices	113
A.	Computation of Side Force Coefficient	115
B.	Variance of a Random Walk Process	117
C.	Pitch Offset Calibration of a Glider	119

D. Proof of Proposition 1	121
E. Sink Rate Polar in Turning	123
Bibliography	127

List of Tables

3.1. Dependencies of the state dynamics on the state variables and measurements.	32
3.2. Technical Data of Glider ASG 29.	43
3.3. Sensor Characteristics	44
3.4. Initialization of the error-state variance. The initial state variances are assumed to be isotropic Gaussian distributed. The value in the table applies to each axis of every 3D state variables.	45
4.1. Simulation parameters for simplified 2D EKF.	59
6.1. Sensor Characteristics and EKF parameters	91
6.2. Impact of the lateral TAS $_{B}v_{t,y}$ on the vertical TAS $_{N}v_{t,z}$	101
6.3. Side force coefficients of different gliders.	103
6.4. Velocities and sideslip angle of a slipping turning of ASG 32.	104
6.5. Test Pilots and Flights.	107

List of Figures

1.1. Energy exploitation of fixed-wing aircraft using local atmospheric turbulence.	2
1.2. 2D example: mean and covariance propagation in EKF and UKF (adapted from [WV00]).	4
1.3. Glider flying in heavy atmospheric turbulence. Photo: Heinrich Meyr.	5
1.4. Glider performance.	6
2.1. Development process of prototyping sensor fusion algorithms.	12
2.2. Wind triangle.	13
2.3. Sensor fusion workbench based on an extended Kalman filter for inertial navigation and wind estimation.	14
2.4. Simulation-in-the-loop: prototyping in MATLAB.	16
2.5. Software-in-the-loop: sensor fusion simulator based on C code.	17
2.6. Overview of the hardware LXNAV S100/S10.	18
2.7. HAWK: on-board implementation of sensor fusion platform.	18
3.1. Aircraft modeling: Euler angles, airspeed ${}_B\mathbf{v}_t$ in the body frame, angle of attack α , sideslip angle β and aerodynamic forces (lift L , drag D and side force Y).	23
3.2. Sensor fusion based on EKF.	29
3.3. Wind triangle ${}_N\mathbf{v}_t = {}_N\mathbf{v} - {}_N\mathbf{d}$	37
3.4. Positive sideslip angle in a right slip. The oncoming airflow comes from the direction of ${}_B\mathbf{v}_t$ acting on the side surface of the fuselage which produces a force F_p . The force F_p has two effects: side force Y and additional drag force F_D	39
3.5. Sink rate residual. Black: polar curve. Blue: the sink rate from the polar is considered as a measurement. Red: the estimated TAS vector results in estimated sink rate. The sink rate residual is defined as the difference between two sink rates.	41
3.6. Generated flight path and attitude of glider ASG 29.	44
3.7. EKF Results for proper initialization.	46
3.8. Euler angles estimates with large initial yaw error.	46

4.1.	Wind triangle: relation between wind, true airspeed and ground speed. . .	50
4.2.	The structure of a Kalman filter [AM12].	55
4.3.	Singular values of the observability matrix at different time instants of the simplified system with the magnetometer.	59
4.4.	SVD of the observability matrix for the 2D model without using a magnetometer [Hua+20]. a) The singular values in a straight and a turning flight, b) The right singular vector \mathbf{v}_6 and \mathbf{v}_1 of the smallest and largest singular value in the straight flight, respectively, c) The right singular vector \mathbf{v}_5 and \mathbf{v}_6 of the two smallest singular values in the turning flight, respectively.	61
4.5.	The smallest singular value versus the rate of change of the heading angle.	62
4.6.	SVD of the observability matrix for the complete EKF with 18 state variables [Hua+20]. a) The six smallest singular values at different time instants, b) The right singular vector \mathbf{v}_{17} and \mathbf{v}_{18} of the second smallest and smallest singular value, respectively.	63
4.7.	Wind estimation under artificial perturbation with and without using a magnetometer [Hua+20].	64
5.1.	(a): Simulated 2D flight path: straight (0 - 94s) and turning (94 - 300s). (b): Eq. (5.34) characterizes the difference of two successive matrices \mathbf{A}_{k+1} and \mathbf{A}_k	74
5.2.	Comparison of the homogeneous state error \mathbf{e}_k , the approximated \mathbf{e}_k^* using the Schur decomposition.	74
5.3.	Example of the system (5.45): (a) Limiting exponential rate in three cases: $\lambda_{12} = 1.5, 2$, and 2.5 . (b) $\lambda_{12} = 1.5$: Exponential rates of the three partitioned components of $\Phi_U(k + k_0, k_0)$	78
5.4.	Norm of the transition matrix $\ \Phi_U\ $ in the ideal simulated flight with a constant heading from 0s to 94s and then turning from 94s to 300s.	80
5.5.	Ideal straight path: (a) The diagonal entries of Φ_U at each time instant k . (b) The 1st row of Φ_U	81
5.6.	Ideal straight path: Euclidean norm of the homogeneous state error, the north and east wind error.	81
5.7.	Simulated flight trajectory: (a) Horizontal path. (b) Heading.	82
5.8.	Norm of the new transition matrix $\ \Phi_U\ $ in the flight with a changing heading.	83
5.9.	Realistic straight path: (a) The diagonal entries of Φ_U at each time instant k . (b) The 1st row of Φ_U	83
5.10.	Perturbed TAS estimate with the wind triangle.	84
5.11.	Acquisition of the state error under perturbed TAS estimate.	84
6.1.	Sink rate polar in straight flight and circling at different roll angles.	88
6.2.	Wind triangle in the vertical axis. Convention of the vertical velocities: upward is positive; downward is negative.	90
6.3.	Accelerometer z-axis measurement: a) raw data b) power spectral density.	91
6.4.	Flight state estimation results of a gliding flight [HMF20].	93
6.5.	IMU bias estimation.	94

6.6.	Standard deviation of the Euler angles and the wind estimates.	94
6.7.	Wind estimation using different wind random walk noise densities σ_d . . .	95
6.8.	Wind along the fuselage of the glider during circling (calculated from the wind triangle). A positive wind means a tailwind. A negative wind presents a headwind. The fuselage aligns with the wind direction twice during one turn, corresponding to the maximum and minimum values at the red and green points, respectively.	95
6.9.	A simple thermal model.	97
6.10.	Estimation results of a typical thermal soaring on the glider ASH-25. The vertical wind, i.e., the local thermal strength, is shown along the curves.	98
6.11.	Horizontal wind flow and average velocity estimates.	99
6.12.	Estimation results before entering a thermal. The vertical wind, i.e., the local thermal strength, is shown along the curves.	99
6.13.	Coordinated, slipping and skidding in a right turning. The yaw string points to the opposite direction of the flight path.	100
6.14.	Uncoordinated turning towards right: (a) Slipping. (b) Skidding.	101
6.15.	Experimental determination of the side force coefficient C_β . The vertical TAS estimate decrease in slipping and increase in skidding with a decreasing side force coefficient	102
6.16.	Vertical wind estimates using different C_β from -0.24 to -0.16 rad^{-1}	103
6.17.	Lift polar: lift coefficient versus angle of attack of airfoil, DU89-134/14, with flap deflection 10° (adapted from [BV97]).	105
6.18.	AoA estimates and related flight variables in (a) a stall flight and (b) a free fall flight [HMF20].	106
7.1.	Development process of sensor fusion algorithms [HMF20].	109
C.1.	Leveling a glider.	119
E.1.	Equilibrium in a level flight (side view of a glider).	123
E.2.	Equilibrium in a turning flight (back view of a glider).	124

List of Abbreviations

AoA	Angle of attack
DLR	German Aerospace Center
EKF	Extended Kalman Filtering
GPS	Global Positioning System
HIL	Hardware-in-the-loop
IMU	Inertial measurement unit
LTI	Linear time-invariant
LTV	Linear time-varying
MEMS	Micro-electro-mechanical systems
NED	North-east-down
PIL	Pilot-in-the-loop
PSD	Power spectral density
SIIL	Simulation-in-the-loop
SIL	Software in the loop
SLAM	Simultaneous localization and mapping
SPKF	Sigma-Point Kalman Filter
STD	Standard deviation
SVD	Singular value decomposition
TAS	True airspeed
TCAS	Traffic Collision Avoidance System
TE	Total-energy
UAV	Unmanned aerial vehicle
UI	User interface
UKF	Unscented Kalman Filter
WGS-84	World Geodetic System 1984

Notation and Symbols

The next list describes symbols and notation that will be later used within the body of the document. Note that the list is not exhaustive. Some symbols with more local scope are not listed.

\mathbb{R}	real numbers
\mathbf{I}	identity matrix
$\mathbf{0}$	zero matrix
\mathbf{A}	uppercase and bold for matrix
\mathbf{a}	lowercase and bold for vector
a, A	scalar value
$\text{diag}[\mathbf{A}]$	diagonal elements of matrix \mathbf{A}
\mathbf{A}^T	matrix transpose
\mathbf{q}_{AB}	quaternion from frame B to frame A
\mathbf{C}_{AB}	coordinate transformation matrix from frame B to frame A
\otimes	quaternion product
\cdot	multiplication
$[\mathbf{a}]_{\times}$	skew-symmetric matrix of a 3×1 vector \mathbf{a}
$\delta \mathbf{x}$	error-state variable
$\bar{\mathbf{x}}$	nominal state variable
$\hat{\mathbf{x}}$	state variable estimate
$\tilde{\mathbf{x}}$	sensor measurement
$\mathbb{E}[\cdot]$	expectation operator
$\text{Cov}[\cdot]$	covariance operator
$\mathcal{N}(\boldsymbol{\mu}, \boldsymbol{\Sigma})$	Gaussian distribution with mean $\boldsymbol{\mu}$ and covariance $\boldsymbol{\Sigma}$
$\mathcal{O}(\cdot)$	higher order term in Taylor expansion
${}^N \mathbf{a}$	vector \mathbf{a} expressed in NED frame
${}^B \mathbf{a}$	vector \mathbf{a} expressed in body frame
${}^S \mathbf{a}$	vector \mathbf{a} expressed in sensor frame
${}^W \mathbf{r}$	GPS position: latitude, longitude and altitude
${}^N \mathbf{d}$	3D wind velocity in NED frame
$\langle \mathbf{a}, \mathbf{b} \rangle$	inner product of vector \mathbf{a} and \mathbf{b}
$\mathbf{n}[\mathbf{a}]$	normalization of vector \mathbf{a}

$L_f^k h$	k th order Lie derivative of nonlinear function h about nonlinear function f
$\ \cdot \ $	Euclidean norm
α	angle of attack
β	sideslip angle
C_β	side force coefficient
p_s	static pressure
p_d	dynamic pressure
v_s	Sink rate of glider speed polar in straight flight
$v_{s,\text{turning}}$	Sink rate of glider speed polar in turning flight

1. Introduction

1.1. Motivation

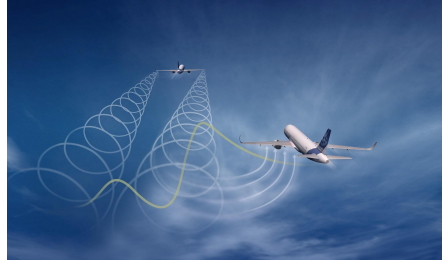
Unprecedented advances in low-cost micro-electro-mechanical systems (MEMS)-based sensors and powerful microprocessors over the past few decades have made the fiction of robotics a reality. For mobility and economic efficiency, manned and unmanned aerial vehicles have been used in a large number of applications such as search and rescue [EEW13], inspection [Den+14], agriculture [Zil+18], parcel delivery [AS18], and urban air mobility [RS20].

Nevertheless, the application of unmanned aerial vehicles (UAVs) faces many challenges, such as limited onboard energy supply. Inspired by birds, the turbulent atmosphere offers opportunities for energy harvesting of fixed-wing airplanes. For example, updrafts and spatially and temporally varying wind fields facilitate soaring for birds and manned gliders. In this regard, precise and real-time local air mass movement is of crucial importance for aerial vehicles to maximize energy gain. Like birds, manned gliders make tight circling in updrafts appearing in narrow columns of rising air to gain altitude. Recently a study carried out by DLR has shown that formation flight can reduce fuel consumption by up to five percent and the climate impact by up to 25% [Luf21]. By imitating migratory birds, airplanes fly in V-shaped formations where the airplanes at the rear can use the vortices produced by those in front. Formation flight requires precise aircraft position and attitude control, which demands reliable and robust estimation of position, attitude, and local air mass turbulence.

The dynamics of aircraft or rotary drones are discussed based on quasi-steady atmospheric conditions assuming small perturbations around steady-state flight conditions [Cau11]. However, the stability and control of aircraft are affected by atmospheric disturbances, including steady wind, wind shear, gusts, and updrafts. These disturbances can be modeled as 3D air mass movement (or wind velocity). From an aircraft's point of view, the atmospheric disturbances are treated as perturbations to the control system and may lead to undesired response dynamics and even instability. Consequently, the disturbances have an impact on the response of the control and estimation system. Therefore, it is necessary to evaluate flight state estimation under representative non-steady atmospheric conditions. Moreover, it is crucial to estimate the 3D wind



(a) Glider ASH 25. Photo: Heinrich Meyr.



(b) The rear aircraft is surfing on wake vortices [Luf21].

Figure 1.1.: Energy exploitation of fixed-wing aircraft using local atmospheric turbulence.

velocity in the flight state estimation.

The successful operation of aerial vehicles requires accurate and robust state estimation providing necessary flight variables for further decision-making procedures. The diversity of applications requires a flexible sensor fusion framework that allows for the rapid transfer of new concepts to implementation in onboard hardware. For the thesis, the focus is placed on the flight state estimation of fixed-wing airplanes.

1.2. Background

Unmanned Aerial Vehicles

UAVs are generally divided into rotary or fixed-wing according to the wing type. Rotary wing UAVs have been widely used in civilian applications like photography due to their low cost, high maneuverability, and lightweight. On the other hand, fixed-wing UAVs have high speed, long-endurance, and a large payload. Either rotary or fixed-wing UAVs are equipped with multiple sensors and actuators. Onboard flight control systems or autopilots perceive real-time sensor signals, compute their state variables and give control commands to actuators.

State Variables

A UAV undergoing six degrees of freedom motion flies in atmospheric turbulence subject to limited onboard measurements. State estimation can enhance the navigation and control capabilities in real flight conditions. The state of an aerial vehicle often refers to a set of variables including three major categories:

1. **Vehicle's motion.** Position, velocity, acceleration, attitude, and angular velocity.
2. **Environmental variables.** Wind speed, pressure at mean sea level, local gravity, air density, and landmark positions.
3. **Sensor calibration related quantities.** Sensor bias, noise, and scale factor.

The state of the system can be a combination of the listed variables, including but not limited to any of the above, which depends on actual applications. In the application of simultaneous localization and mapping (SLAM), the state variables include landmark positions as environmental variables [SSC90]. State estimation is about reconstructing the underlying state of a system using a series of measurements and an a priori model of the system [Bar17]. More important is that it can reconstruct unmeasurable variables such as wind speed.

Sensor

Sensors can be divided into two categories: *interoceptive* and *exteroceptive* [Bar17, Sec. 1.2]. The interoceptive sensors measure quantities relating to stimuli produced within the rigid body. Typical examples include accelerometers that measure acceleration and gyroscopes that measure angular rate. A Pitot tube is used in aviation to measure the aircraft's airspeed. The exteroceptive sensors measure quantities relating to stimuli received by the rigid body from the environment. For example, Global Positioning System (GPS) receivers provide positions in the World Geodetic System (WGS). Vision sensors perceive the range and bearing of landmarks. In avionics applications, pressure sensors are used to measure atmospheric pressure. A magnetometer measures the ambient Earth's magnetic field to derive a heading reference.

Due to cost and weight constraints, the precision of onboard sensors of UAVs and small airplanes cannot be compared to their counterparts used in commercial airlines and military applications. Some of these measurements, like accelerometer and gyroscope, typically are strongly noisy, biased, and scaled [TPM14]. Moreover, GPS measurements are unreliable as due to obstacles (or in indoor environments), the line of sight view to the satellites can be lost. Finally, a magnetometer often provides very imprecise measurements due to disturbance by other magnetic fields nearby [Roe+05b].

Nonlinear Filtering

State estimation is a problem that is nonlinear and complex due to nonlinear kinematics of the aerial vehicle and nonlinear measurement models. In order to tackle the nonlinear estimation, we briefly introduce several nonlinear filtering techniques existing in UAV applications.

A complementary filter comprises a low-pass and a high-pass filter [MHP08]. For attitude estimation, the low-pass filter dealing with accelerometer measurements is complementary to the high-pass filtering on high-frequency gyroscope data [MHP08]. The complementary filter predicts the attitude by integrating angular rates and corrects it based on the gravitational direction from the accelerometer. However, the complementary filter can fail in steep turns since the accelerometer does not measure a bias-free gravitational direction during turning. Therefore, Euston et al. [Eus+08] developed a nonlinear complementary filter with additional airspeed measurements for the attitude estimation in turning. The airspeed measurements are used in a simplified centripetal force model to estimate a bias-free gravitational direction. The filter is designed for UAVs in equilibrium states and is limited in aggressive flight maneuvers like free-fall and slipping. The simple framework specifies that the filter cannot be easily extended

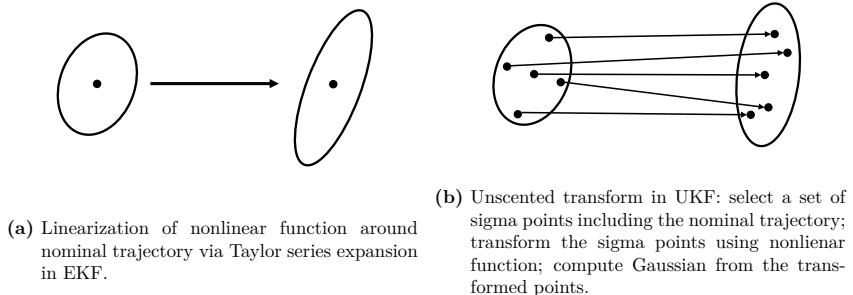


Figure 1.2.: 2D example: mean and covariance propagation in EKF and UKF (adapted from [WV00]).

to include other measurements and state variables. However, the complementary filter is simple and easy to implement on systems with little computational power.

Extended Kalman Filtering (EKF) has been widely used in nonlinear state estimation for robotics [LMS82; Wen+06; BS08; HMR10; Mar11; LS12]. An EKF linearizes the nonlinear system equations and measurement model by a first-order Taylor series expansion around the nominal state trajectory (see Fig. 1.2a). The state estimate is predicted using the nonlinear system equations, and the covariance estimate is propagated using the linearized system equations. Then the state and covariance estimates are updated using the linearized measurement models. Therefore, one of the prerequisites for using EKF is that the linearization errors must be small enough, which requires a high update rate of the EKF. The EKF is proven to be a flexible tool with an extensive heritage that can incorporate a high variety of measurements [CMC07].

In the EKF, the linearization errors can result in sub-optimal performance and sometimes the divergence of the filter [VW04]. To address the issues, Julier et al. [Jul97] developed Unscented Kalman Filter (UKF), also known as Sigma-Point Kalman Filter (SPKF). Instead of linearization of nonlinear equations around the nominal state variables, the UKF calculates a set of sigma points and maps them through the nonlinear equations, as shown in Fig. 1.2b [SE04; Shi06]. Compared to the EKF, the transformed random variables cannot be Gaussian, as shown in Fig. 1.2b. This transformation is called unscented transform and does not require analytical Taylor series expansion of the nonlinear functions [Van04]. Crassidis [Cra06] used the UKF to estimate the position, velocity, attitude, and sensor bias with GPS and inertial measurements. The simulation results showed that the UKF could handle a larger initialization error of the state than the EKF. Considering that the limiting state estimates of the EKF and UKF have the same order of accuracy [RGN13] and that the UKF requires more computational power [Van04], the EKF is a good candidate for sensor fusion framework.

The random variables are assumed to be Gaussian in the EKF, while some camera sensors can produce non-Gaussian noises [STG07]. To deal with non-Gaussian noises and nonlinear system and measurement models, particle filtering is a kind of Monte Carlo

method [Del97] and is used in robotics for low-dimensional systems [Thr02; Bar17]. A particle filter selects a set of samples (particles) to approximate the distribution of a stochastic process given noisy measurements. Each particle is weighted and transformed through the nonlinear system model to approximate the distribution of the posterior stochastic process. Gustafsson et al. [Gus+02] provided a framework for positioning, navigation, and tracking problems based on particle filtering. The particle filter may not be practical in embedded systems with limited processing resources due to the heavy computational load [Shi06].

Atmospheric Disturbances

The definition of atmospheric disturbances is related by their temporal and spatial characteristics and energy content or intensity [Coo12]. In addition, the effect of disturbances on flights also depends on the size and shape of the aircraft, its speed, and altitude [Coo12]. Therefore it is difficult to describe atmospheric disturbances by precise mathematical models adequately. The magnitude of atmospheric disturbances can be classified as light, moderate, severe, and extreme [FAA14]. Here we provide examples of some representative atmospheric disturbances. Fig. 1.3 depicts exemplary heavy atmospheric turbulence during one of our glider flights. For crosswind during take-off and landing, a wind speed less than 5 m/s can be considered as light intensity, while a wind between 5 and 15 m/s is moderate and between 15 and 23 m/s is severe [Coo12].



Figure 1.3.: Glider flying in heavy atmospheric turbulence. Photo: Heinrich Meyr.

Glider Soaring

Gliders take advantage of atmospheric turbulence to maintain and gain height. Vertical wind in a thermal is the primary energy source for gliders. Fig. 1.4a shows a typical glider soaring using a thermal. The pilot optimizes the glide speed and descends until it

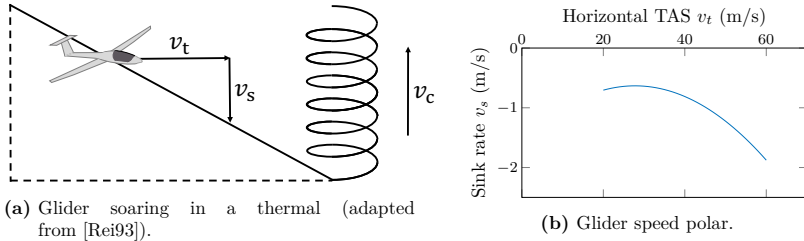


Figure 1.4.: Glider performance.

reaches a point at which there is a strong updraft, then does a circling climb to exploit energy from the air mass.

Speed Polar

In still air, the glider performance can be characterized by its speed polar diagram, which illustrates the horizontal airspeed versus the sink rate, as shown in Fig. 1.4b. The optimum glide speed is determined when the ratio between the horizontal airspeed and sink rate is maximum. Illustratively, this point is the intersection of a tangent starting from the origin to the polar. Note that this optimum glide speed is calculated in still air. In the presence of horizontal wind or vertical wind, the best glide speed must be computed based on adjusted speed polar (see [Rei93] for more details).

Total-Energy Variometer

A total-energy (TE) variometer is a typical instrument equipped on a glider to measure the climb or sink of the vertical air mass movement, i.e., the updraft or the vertical wind speed [Rei93, p. 131]. The vertical air mass movement can be used to indicate the thermal strength and thus impacts the soaring strategy. Initially, a simple variometer only measures the climb rate of the glider by measuring the rate of static pressure change. However, it is impossible to measure updrafts from the glider's climb rate since the climb rate can change due to control, such as pushing or pulling the glider's stick [Rei93].

However, the air mass is not always calm or smooth. For example, in gusty weather, when passing through a wind shear or in the near-ground layer, the airspeed, determined by dynamic pressure, may change suddenly and drastically [Dim03]. In this case, the Pitot tube reacts to a horizontal velocity change caused by gusts. Consequently, the TE variometer displays an erroneous climb or descent of the vertical air mass movement until the glider reaches equilibrium again.

1.3. Outline and Contributions

The overall objective of this thesis is to design, analyze and implement a robust sensor fusion algorithm for flight state estimation of fixed-wing aerial vehicles. Since the kinematic dynamics of aerial vehicles are nonlinear, we study nonlinear state estimation for

inertial navigation systems. Furthermore, we focus on the observability of atmospheric disturbances, i.e., 3D air mass movement, in the sensor fusion framework. We analyze the algorithm in terms of observability, reachability, and tracking behavior. As a user case, we implement the algorithm on commercial avionics devices and use manned gliders for experimental verification and validation. Nevertheless, the developed algorithm is applied to other fixed-wing UAVs.

Outline

Chapter 2 presents a methodology for the design and development of sensor fusion algorithms from concept to inflight testing. First, we define the flight state variables: the position, velocity, attitude of aerial vehicles, accelerometer bias and gyro bias, and 3D air mass movement in terms of wind velocity. The estimation of these variables is tightly addressed in a multisensor framework fusing inertial, pressure, and GPS measurements. The second stage is to identify possible filtering techniques, e.g., we use extended Kalman filtering in the thesis. We develop a toolchain for modeling and simulation of the sensor fusion algorithm. The toolchain includes a prototype in MATLAB and a simulator that is written in C language for embedded applications. Various developing tools are introduced to accelerate the implementation and analysis of the algorithm.

Chapter 3 introduces the mathematical foundations for developing inertial navigation systems and nonlinear filtering. Then, detailed modeling of the system state variables and the measurements are provided. Since the system is nonlinear due to the attitude dynamics, we use error-state modeling of the attitude. The propagation of the error-state model can be approximated as a linear model. The flight state estimation is implemented within an EKF by linearizing and discretizing the nonlinear system around a nominal trajectory. The EKF runs at a sampling rate of 100 Hz, which is larger than the inverse of the dominant time constant of an aerial vehicle in terms of seconds. This estimator is based on the excellent work by Leutenegger [Leu14; Leu+14]. Different from Leutenegger's approach, we do not use a magnetometer since any magnetic materials near the magnetometer lead to a distortion of the local magnetic field and cause errors in the orientation estimation [Roe+05b].

Chapter 4 investigates the observability and reachability of the nonlinear state estimation described in Chapter 3. We use a minimal set of measurements on fix-wing aircraft, including inertial, pressure, and GPS signals. We do not use a magnetometer for heading measurements. The estimation of position, velocity, and attitude has been extensively analyzed in [Cra06; LS12; Sol12; EKK15]. In this chapter, the focus is placed on wind estimation without using a magnetometer based on the concepts of observability and reachability. We first introduce the nonlinear observability and reachability and their application in an EKF. We propose to analyze the observability using singular value decomposition. The singular values imply the observability dimension, whereas the right singular vectors provide detailed information about which state variables are involved in the (un)observable subspaces. For example, we adopt a simplified 2D system estimating 2D position, 2D velocity, and 2D wind velocity with pressure and GPS signals in the measurement update of the simplified 2D EKF. The observability

results show that the 2D wind is observable when the flight heading or the wind changes without a magnetometer. This condition is easily fulfilled in practice, which is verified against measured flight data of a manned glider.

Chapter 5 addresses the dynamic tracking property of the EKF. We first derive the state error transition equation via linearization and discretization of the nonlinear system. Then the dynamic tracking behavior of the state error can be reduced to the stability of a linear time-varying system. In the thesis, we focus on the stability of the deterministic state error, which determines the convergence of the system. We study the convergence of the state error in terms of the Euclidean norm of the transition matrix. This approach gives an overall statement about the stability of the system. In order to investigate the tracking property of individual state variables, we reduce the time-varying system into an upper triangular system via a unitary transformation. The unitary transformation preserves the stability of the original system. The convergence of the system can be seen from the elements in the diagonal of the triangular system. Furthermore, the largest element in the diagonal indicates the dominant time constant of the system. We analyze the dynamic tracking behavior of the simplified 2D EKF using simulated flight data.

Chapter 6 demonstrates the onboard performance of the complete EKF on manned gliders. The focus is on real-time performance in various environmental conditions, including smooth air and the turbulent atmosphere. We show that the flight state variables are well tracked using typical gliding flights. In particular, the EKF can provide 3D real-time wind estimates under atmospheric turbulence. We demonstrate the impact of wind modeling on wind estimation. Furthermore, the EKF is evaluated in uncoordinated turning, stall, and free-fall flights. The flight in uncoordinated turning is used to verify the aircraft modeling, while the stall and free-fall flights show that the EKF can estimate the angle of attack (AoA).

Finally, Chapter 7 summarizes the achievements of this thesis and provides possible directions for future research.

Contributions

In this thesis, we propose an extended Kalman filter using multiple sensors to estimate position, ground speed, orientation, wind speed, and IMU biases for fixed-wing UAVs and airplanes. In order to use the EKF in aviation applications, we develop a toolchain for modeling and simulation of the sensor fusion algorithm. We can develop, implement, and test the EKF in simulation and hardware based on the toolchain.

Due to the nonlinearity of a UAV kinematic system, we linearize and discretize the nonlinear system around a nominal trajectory. The novelty of the EKF is not using the magnetometer or dual GPS, which provides the heading of the UAV. It is crucial to have the heading measurements to differentiate the direction of the ground speed and the true airspeed. However, the magnetometer is sensitive to the local magnetic field of other electric devices. The dual GPS requires the complicated installation of two GPS antennas.

We present an observability analysis of the nonlinear system based on the singular value decomposition. The observability results show that the wind is observable when the flight heading or the wind changes without the heading measurement. Qualitatively, the wind is observable when the rate of change of the heading angle is larger than one degree per second. Due to the random nature of the air mass and the control of the trajectory, the heading fluctuations commonly exist in practical flying. The experimental evaluation of manned gliders shows that the wind estimation does not rely on the magnetometer.

We show that the flight state variables are well tracked using diverse gliding flights. In particular, the EKF can estimate 3D real-time wind under atmospheric turbulence, e.g., thermals and gusts. We compare the 3D wind estimates against a total-energy (TE) variometer measuring the vertical wind. The EKF tracks the vertical wind a couple of seconds faster than the TE variometer. Furthermore, the EKF is not affected by flight maneuvers and gusts. As a byproduct, the EKF is able to track the angle of attack of a fixed-wing airplane, which is verified with stall and free-fall flights.

